Molecular Neurobiology (2022) 59:6076–6090
https://doi.org/10.1007/s12035-022-02947-8

A Functional Interaction Between Y674-R685 Region of the SARS-CoV-2 Spike Protein and the Human α7 Nicotinic Receptor

Juan Facundo Chrestia[1] · Ana Sofia Oliveira[2] · Adrian J. Mulholland[2] · Timothy Gallagher[3] · Isabel Bermúdez[4] · Cecilia Bouzat[1]

Received: 25 March 2022 / Accepted: 28 June 2022 / Published online: 20 July 2022

Abstract

The α7 nicotinic acetylcholine receptor (nAChR) is present in neuronal and non-neuronal cells and has anti-inflammatory actions. Molecular dynamics simulations suggested that α7 nAChR interacts with a region of the SARS-CoV-2 spike protein (S), and a potential contribution of nAChRs to COVID-19 pathophysiology has been proposed. We applied whole-cell and single-channel recordings to determine whether a peptide corresponding to the Y674-R685 region of the S protein can directly affect α7 nAChR function. The S fragment exerts a dual effect on α7. It activates α7 nAChRs in the presence of positive allosteric modulators, in line with our previous molecular dynamics simulations showing favourable binding of this accessible region of the S protein to the nAChR agonist binding site. The S fragment also exerts a negative modulation of α7, which is evidenced by a profound concentration-dependent decrease in the durations of openings and activation episodes of potentiated channels and in the amplitude of macroscopic responses elicited by ACh. Our study identifies a potential functional interaction between α7 nAChR and a region of the S protein, thus providing molecular foundations for further exploring the involvement of nAChRs in COVID-19 pathophysiology.

Keywords Nicotinic receptor · Neurotransmitter receptors · Single-channel recordings · Patch-clamp · SARS-CoV-2 spike protein

Introduction

The spike (S) protein is a homotrimeric type I fusion glycoprotein found on the surface of the severe acute respiratory syndrome coronavirus 2 (SARS-CoV-2) and is composed of two subunits, S1 and S2 (Fig. 1A; Supplementary Fig. 1) [1]. Binding of S1 to the human angiotensin-converting enzyme 2 (ACE2) is essential for the delivery of the viral RNA into the host cell [2, 3], but infectivity is also affected by additional interactions between S1 and the neuropilin 1 receptor [4, 5]. The S protein has been suggested to contribute to COVID-19 pathophysiology also through direct or indirect interactions with other proteins, such as nicotinic acetylcholine receptors (nAChRs) [6–8] and epithelial sodium channels [9].

The interactions between the S protein and nAChRs are thought to occur through the C-terminus region of the S1 subunit (Y674-R685 region) [6]. This region is an exposed loop that contains a motif that is homologous to a motif of snake neurotoxins, which are antagonists of nAChRs, and to a short region of the ectodomain of the rabies virus glycoprotein [6], which has been shown to inhibit ACh-elicited macroscopic currents of α4β2 nAChRs [11].

We recently examined the possible binding of the Y674-R685 region of the S protein to several nAChRs using molecular dynamics (MD) simulations [8]. These simulations predicted favourable binding of the Y674-R685

✉ Cecilia Bouzat
inbouzat@criba.edu.ar

✉ Isabel Bermúdez
ibermudez@brookes.ac.uk

1 Instituto de Investigaciones Bioquímicas de Bahía Blanca, Departamento de Biología, Bioquímica y Farmacia, Universidad Nacional del Sur-Consejo Nacional de Investigaciones Científicas Y Técnicas (CONICET), Camino La Carrindanga Km 7-8000, Bahía Blanca, Argentina

2 Centre for Computational Chemistry, School of Chemistry, University of Bristol, Bristol BS8 1TS, UK

3 School of Chemistry, University of Bristol, Bristol, UK

4 Department of Biological and Medical Sciences, Oxford Brookes University, Oxford OX3 0BP, UK

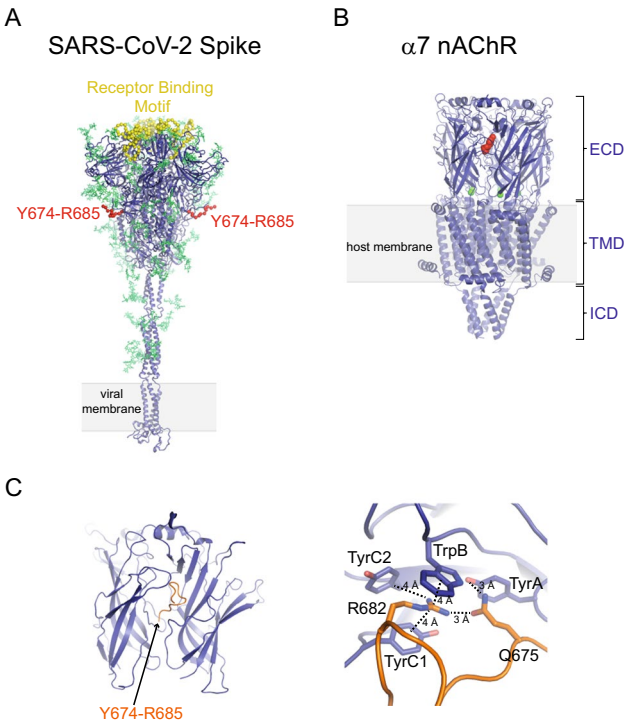

Fig. 1 Three-dimensional structures of the SARS-CoV-2 S protein and the human α7 nAChR. **A** The model represents the complete, fully glycosylated S protein in the closed state after furin cleavage [1]. The protein is rendered as a blue cartoon with the glycans depicted in green. The receptor binding motifs (residues S438-Q506) and the Y674-R685 region are highlighted in yellow and red, respectively. The Y674-R685 region was shown to be accessible for binding in previous MD simulations of the fully glycosylated S protein [8]. **B** Cryo-EM structure of the human α7 nAChR (PDB code: 7KOX) [10]. This receptor is a homopentamer formed of five α7 subunits. Each subunit is composed of an extracellular (ECD), transmembrane (TMD), and intracellular (ICD) domain. The agonist binding site is located in the ECD at the interface between two neighbouring subunits. In this structure, epibatidine (red spheres) is bound to the agonist binding site. The green spheres represent bound calcium ions. **C** MD simulations of Y674-R685 bound to the human α7 nAChR show favourable binding to the binding pocket [8]. Example of conformations from simulations in which the most important interactions with conserved key aromatic residues are present. Left: Overall view of the Y674-R685: α7(ECD) complex. Right: Close-up view of interactions formed by R682 and Q675 within agonist binding site. The α7 receptor and Y674-R685 are coloured in dark blue and orange, respectively. Interactions between side chains of R682 and Q675 and the aromatic rings of TrpB ((α7W171), TyrC1 (α7Y210), TyrC2 (α7Y217) and TyrA (α7Y115) are shown with dashed lines

region to the agonist binding site of the human α4β2 and α7 nAChRs (Fig. 1B, C) and the muscle-like αβγδ receptor from *Tetronarce californica* [8]. Moreover, analyses of the MD simulations of the complete and fully glycosylated S protein showed that the Y674-R685 region is accessible for binding [8]. Among nAChRs, binding of Y674-R685 to the α7 subtype is highly relevant to COVID-19 as nicotine, acting through this receptor, may regulate the expression of ACE2 [12]. Also, activation of α7 nAChR reduces inflammation and tissue damage by downregulating pro-inflammatory cytokines [13–15]. Thus, potentiation of α7 has emerged as an important strategy for modulating inflammation in different pathological contexts, including acute respiratory distress syndrome [13, 16]. Hence, ligands that bind α7 nAChR may affect the SARS-CoV-2 infectivity and the progression of COVID-19. Indeed, recently it has been shown that varenicline, a full agonist at α7 nAChR [17], reduces infectivity and disease progression in a rhesus macaque model [18].

Here, we use whole-cell and single-channel patch clamp recordings to determine whether the Y674-R685 region of the SARS-CoV-2 S protein can directly affect the human α7 nAChR function. Our results reveal that a synthetic peptide corresponding to this region activates α7 in the presence of a potentiator, indicating a functional interaction. Additionally, the Y674-R685 fragment allosterically inhibits α7 nAChR responses at a wide concentration range. This potential functional interaction that we identified may play a role in infectivity and/or disease progression and provides foundations for further exploring the effects of the S protein and other derived fragments on α7 nAChR function.

Materials and Methods

Chemicals

Acetylcholine (ACh) and 5-hydroxyindole (5-HI) were purchased from Merck (USA). PNU-120596 (N-(5-Chloro-2,4-dimethoxyphenyl)-N'-(5-methyl-3-isoxazolyl)-urea) was obtained from Tocris Biosciences (Bristol, UK). Stock solutions were prepared in water (ACh, 5-HI) or DMSO (PNU-120596). The fragment of the S protein (S) of SARS-COV-2, called Y674-R685, contains 12 amino acids with the sequence YQTQTNSPRRAR (MW 1477.60). The peptide was synthesized (90% purity) by Designer Bioscience Ltd. (Cambridge UK) and stored as 1 mM stock solutions (in water) at − 20 °C.

Expression of Human α7 in Mammalian Cells

BOSC-23 cells, derived from HEK-293 cells (kindly provided by Dr. Sine, Mayo Clinic, USA), were cultured with Dulbecco's modified Eagle medium (DMEM) culture medium (GIBCO, USA) supplemented with 100 µg/mL streptomycin-100 IU/mL penicillin (Invitrogen, USA), and 10% Fetal Bovine Serum (FBS, Internegocios, Argentina). Human α7 cDNA subunit (GenBank accession no

X70297.1) was subcloned into the pRBG4 expression vector [19, 20]. BOSC-23 cells were transfected by the calcium phosphate procedure with α7 subunit cDNA together with the α7 chaperones Ric-3 and NACHO cDNAs [21, 22]. The cDNA ratio was 1:2:1 for α7:Ric-3:NACHO, and the total amount was 4.2 µg/35-mm dish. Also, green fluorescence protein (GFP) cDNA plasmid was included to allow the identification of transfected cells [23, 24].

All transfections were carried out for about 8–12 h in DMEM with 10% FBS and terminated by exchanging the medium. Cells were used for experiments 2 to 3 days after transfection, at which time maximum functional expression levels were achieved [19, 25, 26].

Single-Channel Recordings in BOSC-23 Cells

Single channels were recorded in the cell-attached patch configuration at 70 mV pipette potential at room temperature (20–22 °C) [26]. Each patch corresponds to a different cell (n indicates the number of independent experiments). For each condition, at least three different cell transfections from distinct days were performed (N indicates the number of cell transfections).

The bath and pipette solutions contained 142 mM KCl, 5.4 mM NaCl, 1.8 mM $CaCl_2$, 1.7 mM $MgCl_2$, and 10 mM HEPES (pH 7.4). The peptide and 5-HI dissolved in water were added directly to the pipette solution. PNU-120596 in DMSO was added either to the pipette solution or to the dish. The final concentration of DMSO was lower than 0.1% (v/v), which does not affect α7 activation properties [20].

Single-channel currents were digitized at 5–10 µs intervals and low-pass filtered at a cut-off frequency of 10 kHz using an Axopatch 200B patch-clamp amplifier (Molecular Devices, CA, USA). Analysis was performed with the program TAC (Bruxton Corporation, Seattle, WA, USA) with the Gaussian digital filter at 9 kHz (Final cut-off frequency 6.7 kHz) or at 3 kHz for recordings in the presence of PNU-120596. Events were detected by the half-amplitude threshold criterion [26].

Open-time and closed-time histograms were fitted by the sum of exponential functions by maximum likelihood using the program TACFit (Bruxton Corporation, Seattle, WA, USA). The duration of the slowest open component was used for comparisons. Bursts of channel openings were identified as a series of closely separated openings preceded and followed by closings longer than a critical duration, which was taken as the point of intersection between closed components as previously described [25–27]. For α7 activated by ACh, the critical duration for defining a burst was defined by the intersection between the first and second briefest components in the closed-time histogram (~ 200–400 µs). For defining bursts in the presence of 5-HI, critical times were selected between the second and third closed components (~ 1–3 ms) [25–27]. In the presence of PNU-120596 and ACh, α7 nAChR openings are grouped in bursts, and several bursts form long clusters. Each cluster corresponds to the activation episode of the same receptor molecule. For bursts, the critical time was set at 200–400 µs, and for clusters, the critical time was determined by the point of intersection between the third and fourth closed components (~ 30–60 ms) [25]. The burst and cluster durations were taken from the slowest components of the corresponding histograms [25, 26].

Expression of α7 nAChR in *Xenopus laevis* Oocytes

Adult female *Xenopus laevis* were purchased from *Xenopus* One, MI, USA. *Xenopus* care and housing followed the UK Home Office code of practice guidelines for the species. Stage V and VI *Xenopus* oocytes were prepared as previously described [28] and then injected with 2–6 ng of human α7 subunit cDNA into the nucleus in a volume of 23.0 nL, using a Nanoject Automatic Oocyte Injector (Drummond, Broomall, USA). To favour the expression of α7, its cDNA was co-injected with chaperone NACHO cDNA (GenBank accession no BC050273.1) at a ratio of 1 α7: 0.01 NACHO [21, 29]. Injected oocytes were incubated until use at 18 °C in a solution (OR2) containing 82 mM NaCl, 2 mM KCl, 2 mM $MgCl_2$, 5 mM HEPES, pH 7.5, supplemented with 0.1 mg/mL streptomycin, 1000 U/mL penicillin and 100 µg/mL amikacin. Oocytes were used for electrophysiological recordings 1 to 2 days after injection [28, 29].

Electrophysiological Recordings in *Xenopus laevis* Oocytes

Oocytes were impaled with two electrodes filled with 3 M KCl, and the voltage-clamp was maintained at − 60 mV throughout the experiment. All recordings were performed at 18 °C, and cells were perfused continuously with OR2 solution at pH 7.4. Currents were recorded using an automated platform equipped with standard two electrode voltage-clamp configuration (HiClamp; Multi Channel Systems, Reutlingen, Germany). This system differs from standard electrophysiology and other automated platforms because, instead of applying the compound in the perfusion, the oocyte is moved into a well from a 96-well microtiter plate containing 230 µl of the desired solution, as previously described [28]. Experiments were carried out only if the resting potential of the impaled oocytes was greater than − 10 mV and the total holding current less than 0.2 µA.

The ability of fragment Y674-R685 to evoke current responses in *Xenopus* oocytes expressing α7 nAChR was examined at a range of concentrations (1 pM to 10 µM) along with control EC_{50} (100 µM) ACh-evoked responses from the same cells. Compounds were applied for 20 s

and the washout period was 5 min. For experiments that assessed the effects PNU-120596 on the ability of fragment Y674-R685 to activate α7 nAChRs, oocytes displaying maximal ACh current amplitudes of 15–20 μA were used. Our limit of detection for α7 receptor-mediated activity is 0.05–0.08% (10–20 nA of current) of the maximal responses elicited by 1 mM ACh.

To obtain concentration response data for the inhibitory effects of Y674-R685 on α7 nAChRs, a range of concentrations of the fragment (0.1 nM to 30 μM) were co-applied with ACh EC_{50} (100 μM). This concentration range was similar to that used to determine the effects of neurotoxin-like peptides of the rabies virus glycoprotein on nAChRs [11]. The peaks of the current responses obtained in this manner were then normalized to the peak of the responses elicited by ACh alone. The effects of the fragment on the ACh concentration response curve (CRC) were assessed by determining the ACh CRC in the absence and presence of 1 μM Y674-R685. The peak of the ACh responses were normalized to the responses elicited by 1 mM ACh. For both set of studies, the normalized data were fit with the Hill equation using GraphPad software version 5, as previously described [28]. Data are expressed as means ± SEM from 5 to 6 oocytes obtained from at least three different batches of oocytes (N).

Data were filtered at 10 Hz, captured at 100 Hz using proprietary data acquisition software running under Matlab (Mathworks Inc., Natick, MA).

Statistical Analysis

Single-channel data are presented as mean ± SD. Data sets that passed the Shapiro–Wilk test for normality and the Levene Median test for equal variance were analysed using two-tailed Student's *t*-test for pairwise comparisons or Mann–Whitney rank sum test with SigmaPlot 12.0 (Sysat Software, Inc.). Statistically significant differences between two groups of data were established at p values < 0.05. For each condition, n indicates the number of independent experiments, each from different cell patches, and N, the number of cell transfections, each from different days and cell batches.

Results

α7 nAChR Activation by the Y674-R685 Fragment from the SARS-CoV-2 S Protein in the Presence of Potentiators

Our previous MD simulations of the complex formed between the α7 nAChR and the Y674-R685 fragment from the SARS-CoV-2 S protein suggested the potential of the Y674-R685 region to interact with conserved aromatic residues within the binding pocket of the receptor (Fig. 1C) [8]. To establish unequivocally the existence of molecular functional interactions between this region of SARS-CoV-2 S protein and the human α7 nAChR, we evaluated whether the synthetic fragment could elicit macroscopic and high-resolution single-channel currents.

The macroscopic responses of the human α7 nAChR expressed in *Xenopus* oocytes to the applications of the Y674-R685 fragment at a broad range of concentrations (1 pM to 10 μM) were examined along with control ACh-evoked responses from the same cells (Fig. 2A).

As shown in the figure, Y674-R685 did not elicit detectable currents in contrast to the robust responses elicited by 100 μM ACh. After 5-min wash, receptors remained responsive to subsequent control applications of ACh (Fig. 2A).

Single-channel currents from cell-attached patches from BOSC-23 cells expressing human α7 nAChR were also recorded, thus allowing for more detailed mechanistic information. Recordings were carried out in parallel with control experiments with ACh as the agonist to confirm the presence of functional α7 nAChRs in the same batch of cells. ACh (10–100 μM) evoked isolated brief openings (0.1–0.3 ms) or less often short bursts composed of a few openings in quick succession, which correspond to activation of the same receptor molecule [20, 24, 26, 27] (Fig. 2B). In contrast, channel activity was not detected at a range of Y674-R685 concentrations in a total of 21 patches from different cell transfections (1 pM, $n = 3$; 1 nM, $n = 3$; 1 μM, $n = 8$; 10 μM, $n = 3$; 100 μM, $n = 4$) (Fig. 2B).

Given that α7 nAChR activation in the presence of ACh occurs with very low open probability as very brief opening events (Fig. 2B), we sought to explore if the peptide can induce activation in the presence of positive allosteric modulators. Ligands that do not elicit α7 ionotropic activity or do it with extremely low efficacy, but they appear as agonists in the presence of a PAM have been called silent agonists [30–32].

PNU-120596, a type II positive allosteric modulator (PAM), has been extensively used as a tool in α7 nAChR functional studies due to its ability to increase the probability of agonist-elicited channel opening and the open-channel durations and to reduce desensitization [33]. We, therefore, examined whether Y674-R685 elicits α7 channel activity in the presence of PNU-120596. Note that by itself, PNU-120596 cannot induce channel activation [34].

Macroscopic currents elicited by 1 μM Y674-R685 in the presence of 10 μM PNU-120596 were recorded. Under these conditions, currents with amplitudes of 15–20 nA were detected in 30% of the oocytes tested whereas neither Y674-R685 nor PNU-120596 on their own elicited currents ($n = 15$, $N = 3$) (Fig. 3A).

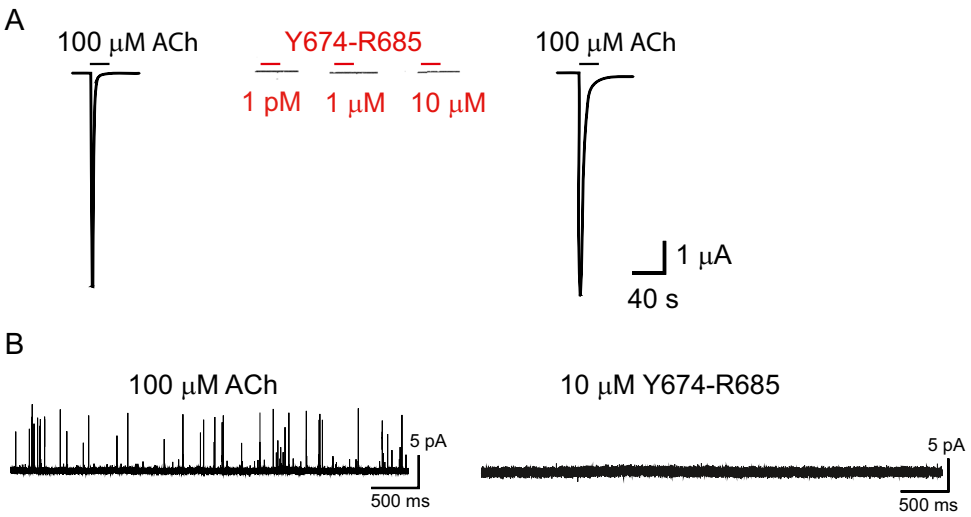

Fig. 2 The Y674-R685 fragment cannot elicit detectable α7 responses. **A** Macroscopic responses of the human α7 nAChR. Representative traces from single oocytes expressing human α7 nAChR to applications of ACh (100 μM) or 1 pM, 1 μM, or 10 μM of Y674-R685. Drug applications were for 20 s followed by a 300 s washout. **B** Single-channel currents of the human α7 nAChR recorded from cell-attached patches in the presence of 100 μM ACh or 10 μM Y674-R685. No channel activity was detected at a 1 pM to 100 μM Y674-R685 concentration range. Channel openings are shown as upward deflections. Pipette potential: 70 mV. Filter: 9 kHz

To gain more insights into how Y674-R685 activates α7 nAChRs in the presence of PNU-120596, we explored its effects at the single-channel level. ACh-elicited activity in the presence of 1 μM PNU-120596 is profoundly different to that in its absence (Fig. 3B). Instead of the brief isolated openings, channel activity shows long periods of high-frequency openings, named clusters, with a mean duration of about 1–3 s and an amplitude of 10 pA (− 70 mV). A cluster corresponds to the activation episode of the same receptor that recovers from desensitization and oscillates between open and closed states before reaching again the more stable non-conducting desensitized state [33]. Clusters are composed of bursts with mean durations of ~ 200–500 ms, which comprise successive openings separated by very brief closings (Figs. 3B and 4) [25, 33].

In the presence of 1 μM PNU-120596, Y674-R685 was capable of eliciting channel activity at a wide range of concentrations (1 pM to 10 μM), indicating that this fragment of the S protein can activate α7 nAChRs in the presence of the PAM (Fig. 3B). Since the frequency of channels is variable among patches due to variations in receptor expression levels, parallel control recordings in the presence of ACh were made. When ACh and PNU-120596 were co-applied, > 98% of patches showed channel activity (active patches), and the long-duration clusters described above appeared at high frequency as reported before [23] (Fig. 3B). In the presence of PNU-120596 and Y674-R685, the percentage of active patches was lower than in the presence of ACh: 65% ($n = 23$, $N = 4$; 1 pM Y674-R685), 40% ($n = 15$, $N = 4$; 1 nM Y674-R685), 67% ($n = 15$, $N = 4$; 1 μM Y674-R685), and 62% ($n = 13$, $N = 3$; 10 μM Y674-R685). Also, channel activity evoked by Y674-R685 (in the presence of the PAM) was much more infrequent and interspaced by longer silent periods when compared to that evoked by ACh (Fig. 3B). It is important to note that this type of experiments does not allow for a precise comparison of channel frequency since this parameter may be affected by the variability in the number of receptors in each patch. Nevertheless, at 1 pM Y674-R685, the frequency of channel activation episodes was very low, albeit the active patches showed long clusters resembling those elicited by ACh and PNU-120596 (Figs. 3B and 4). The fact that the Y674-R685 fragment activates α7 only in the presence of a PAM suggests that it may act as a silent agonist [31, 32].

The channel activity pattern is similar between ACh and 1 pM Y674-R685 fragment (both in the presence of PNU-120596). The increase in Y674-R685 concentration resulted in profound changes in this pattern, as clearly illustrated in the recordings shown in Fig. 3B. The frequency of opening events appeared to increase, but the duration of the openings and the activation episodes were reduced with increasing concentrations. The typical long-duration clusters were completely absent at Y674-R685 concentrations higher than 1 μM, at which activation occurred mainly as isolated openings or in short bursts (Figs. 3B and 4).

To define the properties of the activation episodes elicited by the Y674-R685 fragment at different concentrations, the mean durations of openings, bursts, and clusters in the presence of PNU-120596 were determined (Fig. 4). At 1 pM Y674-R685, the mean durations of the slowest

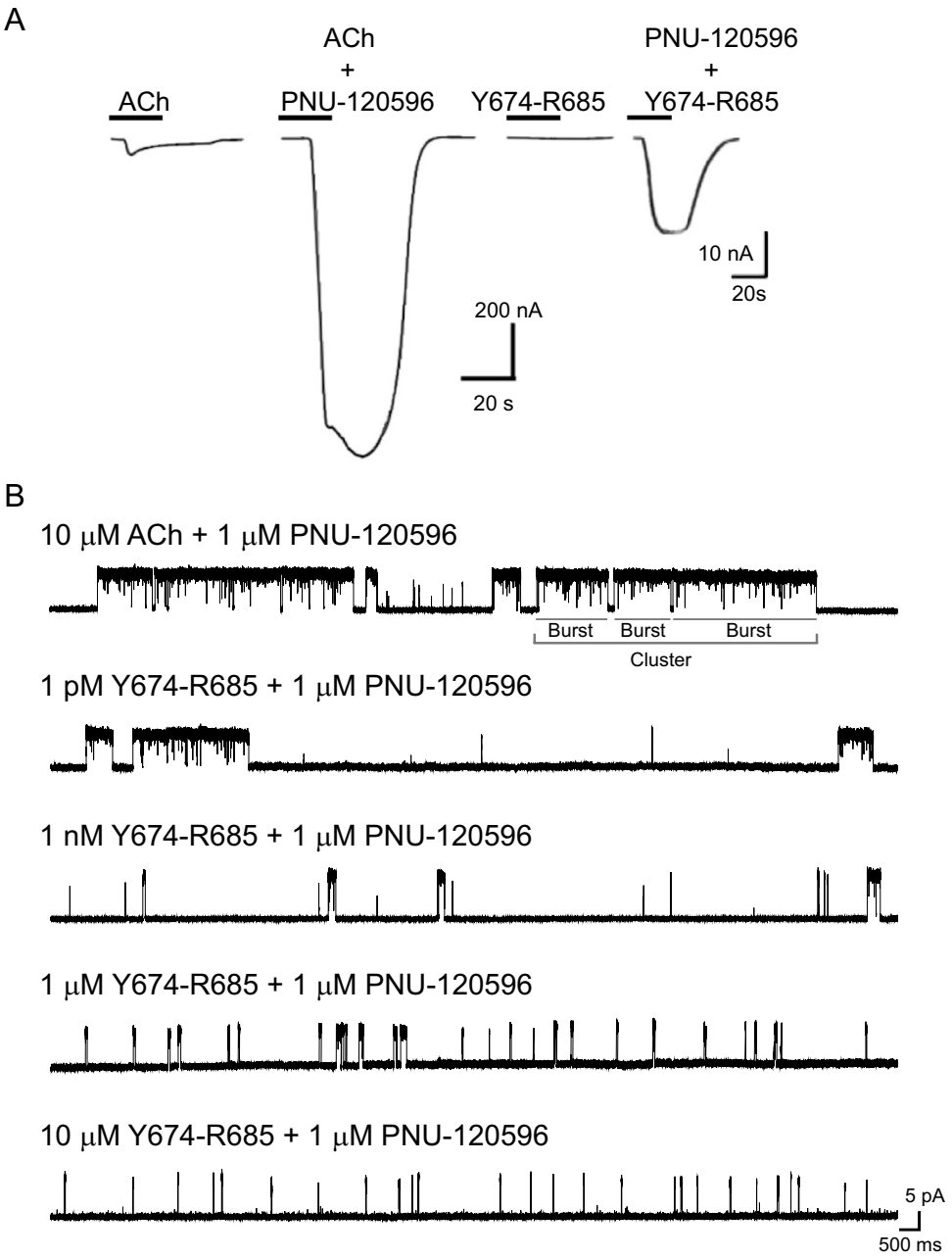

Fig. 3 Activation of the human α7 nAChR by Y674-R685 in the presence of the PAM PNU-120596. **A** Macroscopic currents were recorded from oocytes expressing the human α7 nAChR after a pulse of 30 μM ACh (control) or 1 μM Y674-R685 in the absence or presence of 10 μM PNU-120596. Current traces shown are representative of $n = 15$ recordings from oocytes isolated from N = 3 donors. **B** Single-channel currents of the human α7 nAChR in the presence of the type II PAM PNU-120596 (1 μM) activated by 100 μM ACh (left), or Y674-R685 at different concentrations (1 pM, 1 nM, 1 μM, or 10 μM) (right). For each condition typical channel traces are shown. Channel openings are shown as upward deflections. Pipette potential: 70 mV. Filter: 3 kHz

open component, bursts and clusters were 140 ± 60 ms, 418 ± 110 ms, and 2330 ± 670 ms, respectively ($n = 3$). These values were similar to those determined when 10 μM ACh was the agonist: 148 ± 12 ms for the slowest open component ($p = 0.85$, $n = 3$), 550 ± 38 ms for bursts ($p = 0.12$, $n = 3$), and 3048 ± 510 ms for clusters ($p = 0.21$, $n = 3$), and also comparable to those reported before for 100 μM ACh and 1 μM PNU-120596 [25, 33]. Although the mean durations of clusters were similar at 10 μM ACh and 1 pM Y674-R685, the relative area of the components corresponding to clusters in the histogram was smaller when Y674-R685 was the agonist (relative areas were for ACh = 0.44 ± 0.09 and for Y674-R685 = 0.21 ± 0.08; p = 0.03) (Fig. 4), indicating a reduction in the frequency of the long activation episodes.

With the increase of Y674-R685 concentration, the durations of open, bursts, and clusters were reduced (Fig. 3). The slowest component of each histogram became progressively briefer with increasing Y674-R685 concentrations (Fig. 4). The mean durations were 48 ± 13 ms (1 μM, $n = 3$) and 14 ± 4 ms (10 μM, $n = 4$) for openings; 70 ± 19 ms (1 μM, $n = 3$) and 20 ± 8 ms (10 μM, $n = 4$) for bursts; and 104 ± 41 ms (1 μM, $n = 3$) and 30 ± 15 ms (10 μM, $n = 4$) for clusters. These mean values were statistically significantly different to those determined in the presence of 10 μM ACh

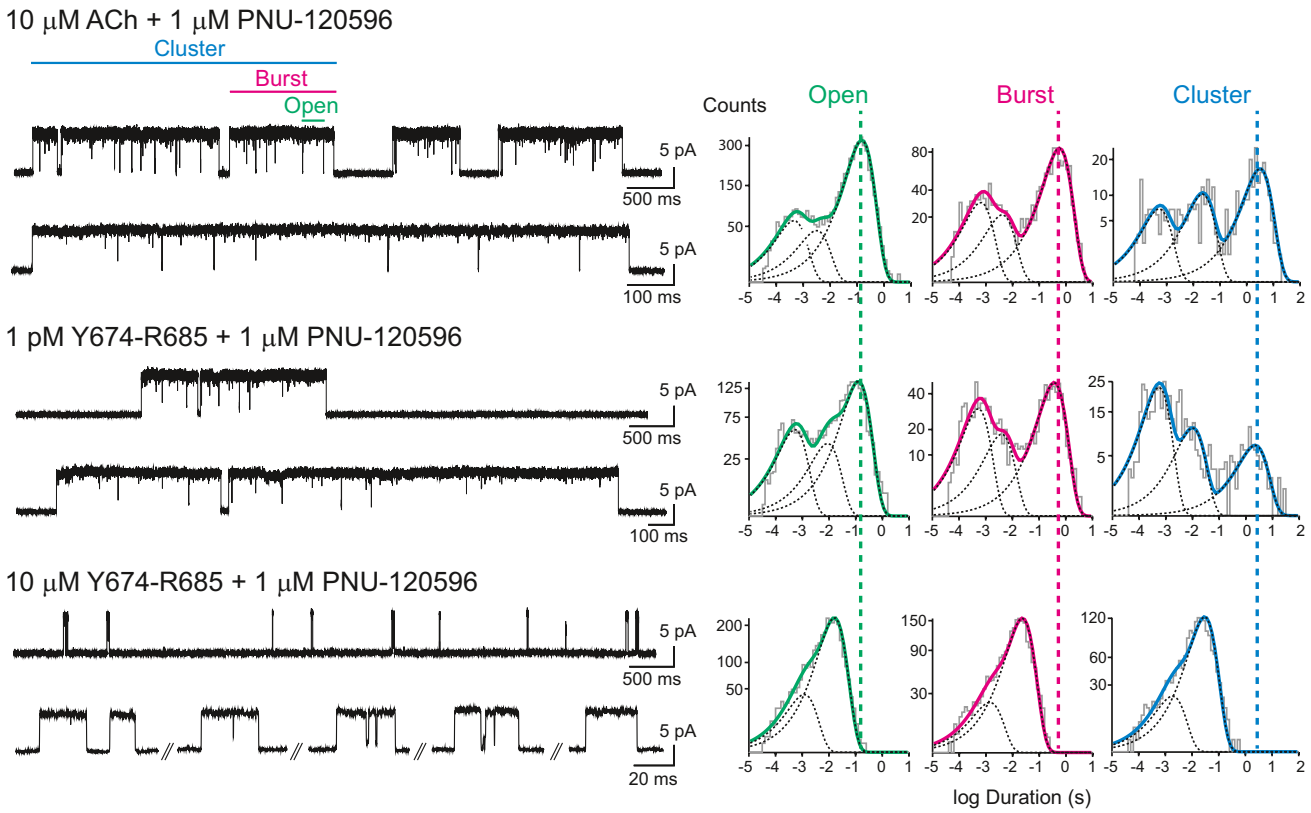

Fig. 4 Single-channel recordings of the human α7 nAChR in the presence of Y674-R685. Single-channel currents of human α7 nAChR in the presence of the type II PAM PNU-120596 (1 μM) activated by 100 μM ACh, or Y674-R685 at 1 pM or 10 μM. For each condition, channel traces at two different temporal scales are shown. Channel openings are shown as upward deflections. Representative open, burst, and cluster duration histograms are shown for each condition. The open, burst, and cluster durations correspond to the durations of the slowest components of each histogram. The dashed lines show how these mean durations change among different conditions. Pipette potential: 70 mV. Filter: 3 kHz

and 1 μM PNU-120596 ($p = 0.000665$ and $p = 0.00000431$ for open; $p = 0.0000403$ and $p = 0.00000106$ for bursts; $p = 0.000597$ and $p = 0.0000681$ for clusters, for 1 and 10 μM Y674-R685, respectively). At the highest Y674-R685 concentration (10 μM), the mean open duration was similar to the mean burst and cluster durations (Fig. 4), indicating that openings occurred mostly in isolation and confirming the lack of the typical long-duration clusters corresponding to potentiated α7 nAChR responses.

To further confirm that channel activation can be elicited by Y674-R685 in the presence of PNU-120596 but not in its absence a different strategy was followed. Single-channel recordings in the presence of different concentrations of the Y674-R685 fragment (1 μM and 10 μM) were performed. Again, no channel activity was detected in all patches ($n = 9$, $N = 2$). However, the addition of 1 μM PNU-120596 to the dish during the course of the recording resulted in the appearance of single-channel activity in most of the silent patches (83.3% and 100% for 1 μM ($n = 6$) and 10 μM Y674-R685 ($n = 3$), respectively) (Fig. 5). Since this strategy allows comparison of both conditions (with and without PNU-120596) in the same patch, it confirms that activation by Y674-R685 requires the PAM. The same strategy applied using ACh as the agonist showed that the typical brief isolated openings were replaced by long-duration clusters after addition of PNU-120596 (Fig. 5, [33]. The frequency of opening events was markedly lower, and the durations were briefer at 10 μM Y674-R685 with respect to the recordings with ACh (Fig. 5).

Together, these results confirm that Y674-R685 functionally interacts with the α7 nAChR. They show that the Y674-R685 peptide activates the receptor only in the presence of PNU-120596, and that the increase in its concentration is accompanied by a decrease of the duration of open channel lifetime and clusters.

Because PNU-120596 is a highly efficacious type II PAM with the capability of recovering receptors from desensitization, we also tested if Y674-R685 elicited channel activity in the presence of 5-hydroxyindole (5-HI), a type I PAM. This compound induces potentiation with lower efficacy than PNU-120596 and does not produce significant recovery of receptors from desensitization [24, 25, 35]. In the

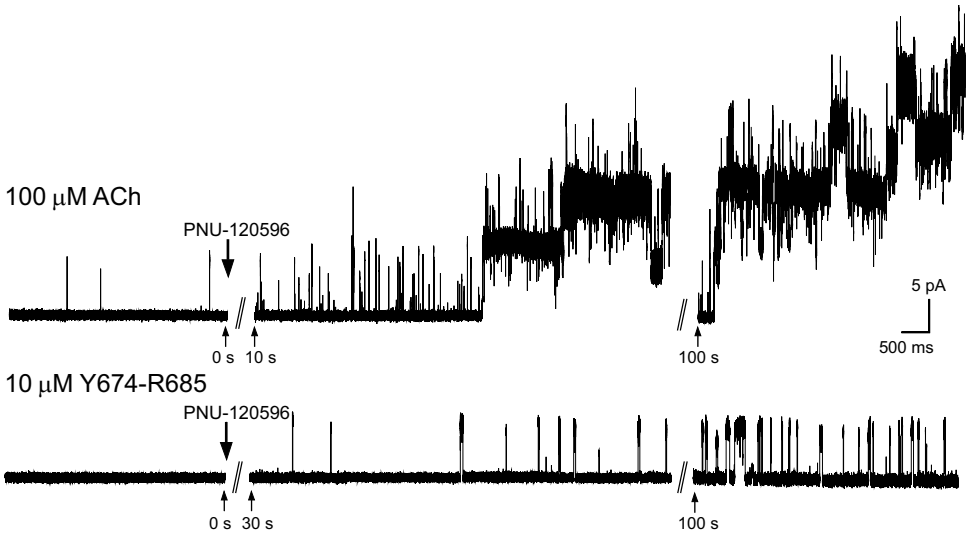

Fig. 5 Channel activity elicited by Y674-R685 in the absence or presence of the PAM. Representative experiments in which channel activity from the same patch was recorded before and after addition of PNU-120596. ACh or 10 μM Y674-R685 were present in the pipette solution. The indicated time corresponds to the time of recording after addition of PNU-120596. Top: single-channel currents of human α7 activated by 100 μM ACh appeared mainly as brief isolated openings. Addition of 1 μM PNU-120596 to the extracellular solution surrounding a cell-attached patch resulted in a marked increase in current in the continued presence of 100 μM ACh in the patch pipette. This experiment is representative of 4 different patches. Bottom: channel activity was undetectable in the presence of Y674-R685. Addition of 1 μM PNU-120596 to the extracellular solution surrounding the silent patch revealed channel activity, indicating that only in the presence of the PAM 10 μM Y674-R685 can activate α7. This experiment is representative of 3 different patches. Channel openings are shown as upward deflections. Pipette potential: 70 mV. Filter 3 kHz

presence of 2 mM 5-HI, 100 μM ACh elicited prolonged openings and bursts composed of successive openings which lasted about 4 ms (Fig. 6). The histograms showed that the duration of the slowest open component was fourfold longer (1.28 ± 0.35 ms, $n = 37$, versus 0.30 ± 0.06 ms, $n = 38$) and the mean burst duration was eightfold longer (3.60 ± 1.29 ms, $n = 37$, versus 0.46 ± 0.12 ms, $n = 38$) than in the absence of the PAM. Replacing ACh by Y674-R685 (1 pM or 10 μM) revealed α7 channel activity. However, the frequency of opening events was markedly lower when compared to that elicited by ACh; only few events were detected during a 15-min recording period (Fig. 6). At 1 pM Y674-R685, 83.3% of the patches showed α7 channel activity, but the frequency of openings was very low ($n = 18$, $N = 3$). We therefore combined all recordings for constructing open and burst duration histograms. The resulting mean open and burst durations were 1.1 ms and 4.2 ms, respectively (Supplementary Fig. 2). At 10 μM Y674-R685, the frequency of channel openings was higher than at 1 pM but still lower than that elicited by ACh. The mean open and burst durations were 0.73 ± 0.07 ms and 0.85 ± 0.13 ms ($n = 3$), respectively. Both mean durations were statistically significantly briefer than the corresponding ones in the presence of ACh and 2 mM 5-HI ($p = 0.0114$ and 0.005 for mean open and mean burst durations, respectively). Also, the observation that in the presence of 2 mM 5-HI and 10 μM Y674-R685 the mean duration of openings was similar to that of bursts indicates that at high fragment concentrations channel openings occurred mainly as isolated events instead of in quick succession forming activation episodes, as described before for recordings with the type II PAM PNU-120596.

Inhibition of α7 Activity by the Y674-R685 Peptide

To further explore the molecular mechanisms driving the inhibitory effects of the Y674-R685 fragment, we studied its action on α7 activated by ACh, which allows recordings of higher channel activity than with the peptide as the agonist (Fig. 7A). Given the very brief open duration of α7 channels, which is close to the time resolution of our system, we needed to include PNU-120596 to quantify the decrease in open durations.

Whereas in the presence of 1 μM PNU-120596, 10 μM ACh led to an activation pattern composed of long clusters as described above, the inclusion of Y674-R685 produced marked changes in this pattern in a concentration-dependent manner (Fig. 7A and Supplementary Table 1). The results showed that the cluster duration was the most sensitive parameter. With respect to the control recordings with ACh and PNU-120596, the presence of 1 pM and 1 nM Y674-R685 reduced the cluster duration 72% and 78%, respectively, and the open duration 54% and 57%, respectively (Fig. 7A, Supplementary Table 1). As

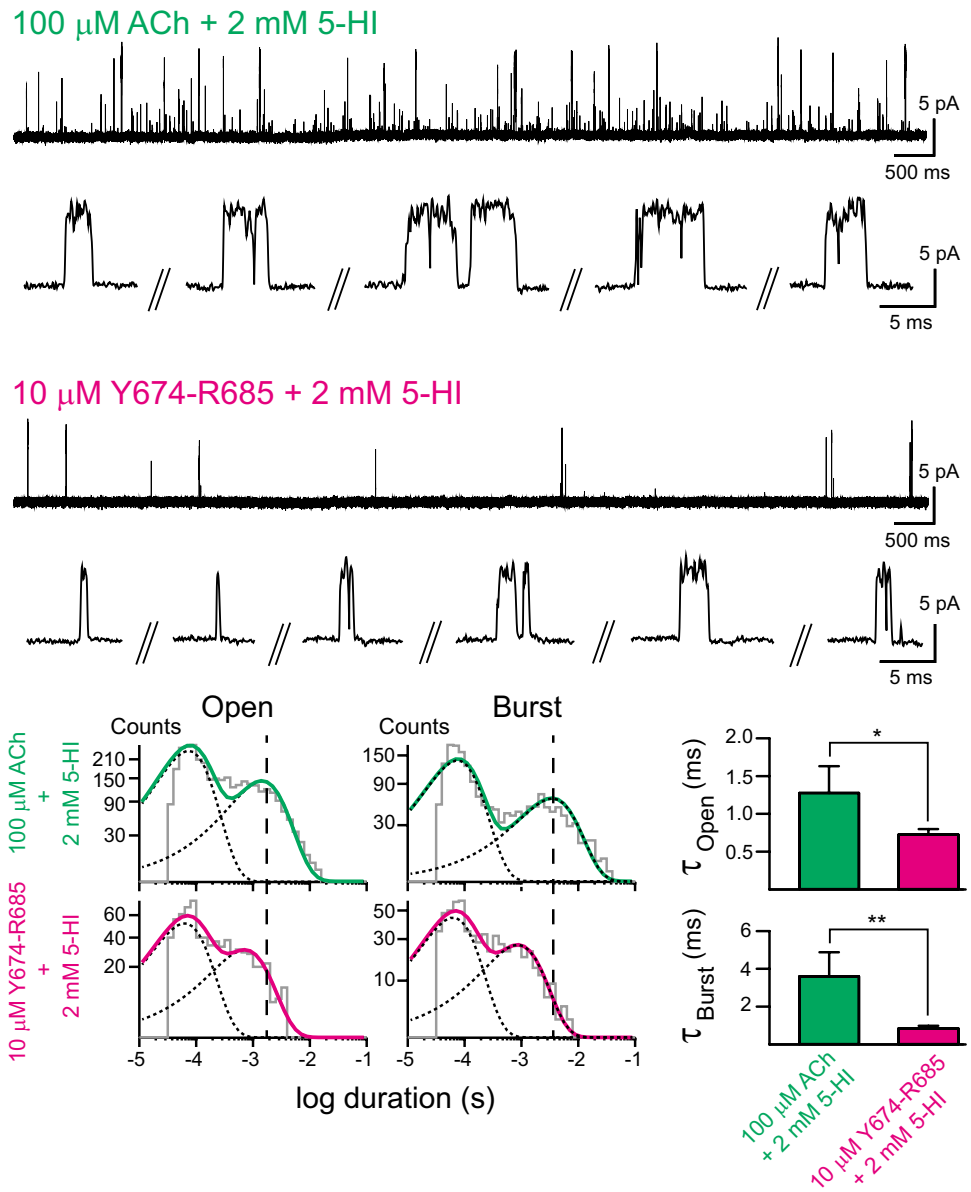

Fig. 6 Activation of the human α7 nAChR by Y674-R685 in the presence of the type I PAM, 5-HI. Single-channel currents were recorded from cells expressing the human α7 nAChR in the presence of 2 mM 5-HI as the PAM and 100 μM ACh or 10 μM Y674-R685 as agonists. Traces at two different scales are shown for each condition. Pipette potential: 70 mV, Filter: 9 kHz. Representative open and burst duration histograms are shown for each agonist. The bar chart shows the mean durations ± SD of the slowest components of the open and burst duration histograms for each agonist ($n = 37$ for ACh and $n = 3$ for Y674-R685). *$p < 0.05$, **$p < 0.01$ (Student's *t*-test)

the concentration increased, the inhibition was more evident and at 10 μM Y674-R685, the long durations clusters were absent, and only markedly briefer bursts were detected (Fig. 7A and Supplementary Table 1). At this high concentration, the mean duration of the slowest open component was 9.9 ± 2.6 ms ($n = 4$), which corresponds to about 7% of the control open duration. Also, the open duration was not different from the mean burst duration (11.2 ± 3.0 ms, $n = 4$), indicating that most long openings occurred in isolation (Supplementary Table 1). Although clusters were not visually detected, we constructed cluster duration histograms using a critical time for cluster resolution between 10 and 20 ms, which is about 20 to 40-fold times longer than that used for burst-duration histograms. The mean duration of the slowest component of the cluster histogram was 14.1 ± 4.4 ms ($n = 4$), which was similar to that of bursts, thus confirming the lack of the long-duration activation episodes occurring in potentiated α7 channels in the presence of 10 μM Y674-R685 (Fig. 7A, Supplementary Table 1).

We also analysed dwell times in the closed state as a function of different peptide concentrations of channels elicited by ACh in the presence of PNU-120596. For the control condition (no peptide), histograms were fitted by five or six exponential components. The three briefest components correspond to intracluster closings and their mean durations were constant among different recordings (Supplementary Fig. 3). The two or three slowest closed components correspond to closings separating clusters, isolated bursts, or isolated openings and showed variable durations among patches due to differences in receptor expression levels. The

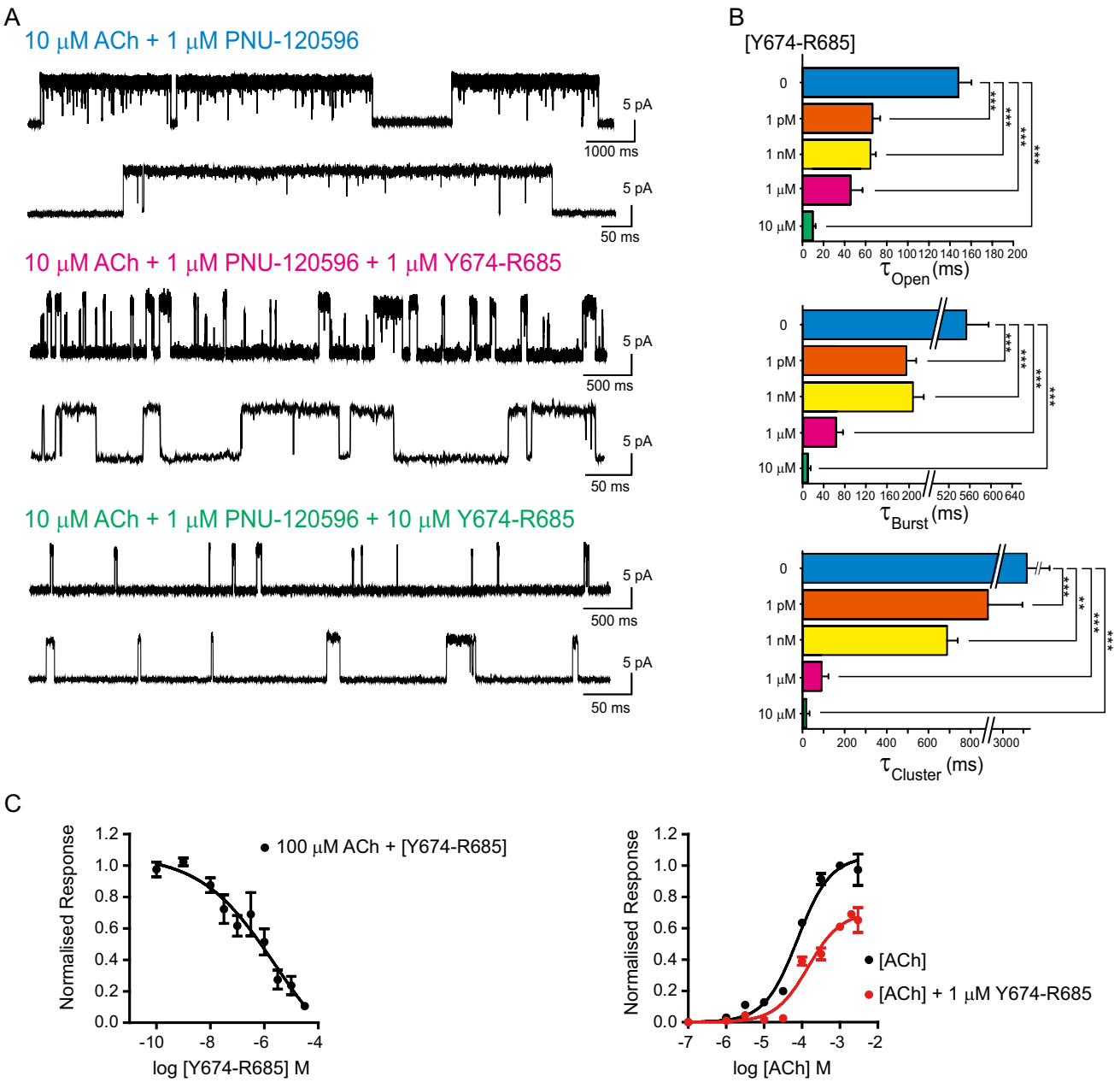

Fig. 7 Y674-R685 Inhibition of α7 nAChR channels activated by ACh. **A** Single-channel currents elicited by 10 μM ACh and potentiated by 1 μM PNU-120596 were recorded in the absence (control) or presence of 1 or 10 μM Y674-R685. Typical channel traces are shown at two different temporal scales. Channel openings are shown as upward deflections. Pipette potential: 70 mV. Filter: 3 kHz. **B** Bar chart showing the mean durations of openings (τopen), bursts (τburst), and clusters (τcluster) in the absence (blue) and in the presence of 1 pM (orange), 1 nM (yellow), 1 μM (pink), and 10 μM (green) Y674-R685. The data correspond to the mean duration (±SD) of the slowest components of open, burst, and cluster histograms. $^{**}p<0.01$, $^{***}p<0.001$ (Student's *t*-test) (see Supplementary Table 1). **C** Concentration response curve (CRC) for the inhibition of the α7 nAChR by Y674-R685**.** Increasing concentrations of Y674-R685 (0.1 nM to 30 μM) were co-applied with control ACh (100 μM). Responses were measured from the peak of ACh-elicited currents. Each data point represents the average normalized response of six cells (±SEM). *Right panel*: competition CRC data (red) for 1 μM Y674-R685 co-applied with different ACh concentrations (0.1–2000 μM). For comparison, ACh CRC data alone (black) are shown at the same concentrations. Data were fitted with the Hill equation, as described in the "Materials and methods" section. Data points represent the average normalized response of six oocytes (±SEM)

briefest component is the major component and corresponds to closings between openings that occur at a high frequency within clusters. With the increase of peptide concentration, the area of the briefest closed component decreased (from about 64 to 24% at 10 μM) and the slowest component became the predominant one (Supplementary Fig. 3). This

slowest closed component at the highest peptide concentrations showed variable mean durations among recordings. Comparisons of closed time histograms among recordings with different peptide concentrations did not reveal any new component of constant duration whose area increased with the peptide concentration.

To explore possible inhibitory mechanisms, we analysed our findings on the basis of a simple open-channel block mechanism [36]. Hallmarks of a simple open-channel block mechanism are as follows: (i) decrease in mean open time as a function of blocker concentration, (ii) concentration-dependent increase in the fractional area of the blocked component, (iii) constant mean duration of the blocked period across blocker concentrations, and (iv) increase of the burst duration as a function of the blocker concentration [36]. Our recordings in the presence of PNU-120596 and ACh showed a decrease in open duration as a function of peptide concentration, which may suggest open-channel block. However, they showed a decrease in the cluster duration and did not show any flickering, typical of fast open-channel blockers [36]. Also, the closed time histograms did not reveal any new component that may be unequivocally assigned to a blocked period.

To gain further insight into the mechanism driving the inhibitory effect of Y674-R685 in the presence of ACh and PNU-120596, we compared the pattern of channel activity when methyllycaconitine (MLA), a reversible competitive α7 antagonist [17], was present instead of the S fragment. To better assess the impact of MLA, we used the strategy of filling the tip of the pipette with the buffer solution containing 10 µM ACh and 1 µM PNU-120596 and the shaft with the same solution but including MLA (100 nM). This strategy allowed following in real-time the effects of the antagonist during the recording of ACh-activated channels. While at the beginning of the recording the typical pattern comprising high-frequency channel activity and long duration clusters was observed, channel activity decreased over time and was completely suppressed after about 10–15 min due to the presence of MLA (Supplementary Fig. 4, $n=3$). No reduction in the duration of clusters or bursts, as described in the presence of Y674-R685, was detected in the presence of MLA (Supplementary Fig. 4). Thus, the type of inhibition mediated by Y674-R685 differs from that produced by the competitive antagonist.

The results together suggest that the Y674-R685 region of the S protein acts as a non-competitive antagonist of α7. To further confirm this result, we determined the effects of Y674-R685 on the peak current responses evoked by an approximate EC_{50} concentration of ACh (100 µM). Application of Y674-R685 with ACh inhibited peak currents, with an IC_{50} of 1.8 ± 0.8 µM ($n=10$), but inhibition was not complete (Fig. 7B). We then investigated whether the observed antagonism was competitive or not. For these studies, 1 µM Y674-R685 was co-applied with increasing concentrations of ACh (0.1–2000 µM) (Fig. 7B). Compared to ACh alone, Y674-R685 co-application affected ACh efficacy, reducing the maximal currents elicited by ACh (Imax) by $30 \pm 4\%$ ($n=6$) and slightly affecting its potency ($EC_{50}=80 \pm 6$ µM and 131 ± 92 µM) ($n=6$). These results confirm the non-competitive antagonism of ACh responses by Y674-R685.

Discussion

Here, we provide molecular evidence of a direct functional interaction between the human α7 nAChR and a synthetic peptide corresponding to the Y674-R685 region of the SARS-CoV-2 S protein. This interaction, which takes place within the picomolar to micromolar concentration range, results in a dual effect involving activation in the presence of a PAM and non-competitive antagonism. These results agree with our previous MD simulations showing a possible interaction between the Y674-R685 region in the intact (furin cleaved and fully glycosylated) S protein [8] and open doors for further exploring α7 nAChR-S protein interactions.

α7 is a homomeric nAChR highly expressed in both neuronal and non-neuronal cells, which is emerging as a potential drug target for neurological, neurodegenerative, and inflammatory disorders [37–39]. It responds to ACh by opening an intrinsic ion channel permeable to cations, triggering rapid membrane depolarization and calcium influx [40]. α7 activation is unique as it shows low probability of opening, extremely rapid desensitization and very high calcium permeability [41, 42]. We found that the Y674-R685 peptide activates the α7 receptor at picomolar concentrations but only in the presence of PAMs.

PAMs reduce the energy barrier for activation and are emerging as novel therapeutic tools for neurological, neurodegenerative, and inflammatory disorders as they potentiate α7 responses in the presence of an agonist [37, 38, 43, 44]. They have been classified as type I PAMs, which enhance agonist-induced macroscopic currents, and type II PAMs, that also delay desensitization and recover receptors from desensitized states [25, 45, 46]. At the single channel level, PAMs enhance open channel durations and induce activation in episodes in which the channel oscillates between open and closed conformations, thus generating an activity pattern markedly different from the isolated sub millisecond-openings in the absence of PAMs [25]. The Y674-R685 fragment activates the α7 nAChR in the presence of both PAMs, although activation is significantly more efficacious in the presence of PNU-120596 than 5-HI.

Ligands that do not elicit α7 nAChR channel opening but appear as agonists in the presence of a PAM have been recently named as silent agonists [30, 32, 47]. It has been

reported that this type of ligands may be effective desensitizers and may elicit α7 nAChR metabotropic responses, which include release of calcium from intracellular stores and triggering signal transduction pathways [13, 40, 48, 49]. It has been suggested that α7 nAChR silent agonists may be used for the treatment of inflammatory disorders since α7-metabotropic activity is particularly important in immune cells [50]. This raises important questions regarding how α7 metabotropic responses are modified by the S fragment and S protein and the impact on COVID-19 pathophysiology, which call for further studies.

The ability to activate α7 (in the presence of a PAM) is consistent with data from our MD simulations predicting that Y674-R685 can bind directly to the agonist binding site located in the extracellular domain of the α7 nAChR, leading in some conformations to a semi-capped loop C [8]. Loop C is one of the three loops that form the principal face of the orthosteric binding site [10]. Upon agonist binding, loop C closes to cap the agonist, an event associated with priming and channel opening [51]. Loop C capping aids the anchoring of the bound agonist to the orthosteric binding site. It has also been suggested that agonists induce more compact loop conformations, while partial agonists and antagonists produce incomplete closure or prevent loop C capping [52–54].

Our previous MD simulations of Y674-R685 bound to the α7 nAChR identified the guanidinium group of R682 in the SARS-COV-2 S protein as the key anchoring point to the α7 nAChR (Fig. 1C), forming strong interactions with several residues lining the receptor's ligand binding pocket [8]. These simulations also show that, when bound to α7, the Y674-R685 region of the S protein adopts many different conformations within the binding pocket, ranging from highly compact to fully extended configurations (Supplementary Fig. 5). Some of these binding modes allow for the formation of the key interactions necessary to activate the receptor (Fig. 1C), while others do not (Supplementary Fig. 6) [8]. Although the α7 nAChR has five identical orthosteric binding sites, agonist occupancy of only one is required to elicit channel activation [27]. Thus, it could be possible that the Y674-R685 fragment occupancy of the binding sites in multiple orientations, some of which cannot trigger activation, may contribute to its low efficacy, as described before for partial agonists [54]. Alternatively, the partial closure of loop C in the presence of the Y674-R685 [8] observed in some of our previous simulations may also reduce the efficacy for channel opening (Supplementary Fig. 7).

In addition to the activation of α7, the S fragment also shows a concentration-dependent inhibitory action. At 1 pM Y674-R685, channel activity in the presence of PNU-120596 is markedly infrequent but kinetically indistinguishable from the ACh-elicited one. The open channel lifetime and the architecture and duration of the activation episodes (clusters) are similar in the presence of ACh or 1 pM Y674-R685. As the Y674-R685 concentration increases, the frequency of opening events increases, but their durations become progressively briefer and long-duration clusters are not detected. This inhibitory effect was confirmed by experiments in which ACh was the agonist, clearly showing a concentration-dependent reduction of open, burst and cluster durations by the Y674-R685 fragment. The changes in the channel activity pattern were completely different to those mediated by MLA, suggesting different mechanisms. The classical pharmacological experiments using dose–response curves from macroscopic current recordings support an additional mechanism of non-competitive inhibition exerted by the S protein fragment.

As shown here for Y674-R685, several compounds of different structures have dual opposite effects on nAChRs, including α7, by acting as agonists and non-competitive antagonists [23, 55, 56]. Allosteric sites may be located in different receptor domains, including the extracellular and transmembrane domains and channel pore [33, 44, 57, 58]. The site(s) from which the Y674-R685 peptide exerts inhibition as well as the precise mechanism(s) remain to be determined. The main change at the single-channel level is the decrease in the cluster duration to such an extent that at a peptide concentration of 10 μM clusters are no longer detected, and only isolated short bursts or openings are observed. In addition, a new closed component corresponding to block is not detected. Thus, the changes in channel activity as a function of the peptide concentration are inconsistent with its action as a simple fast open-channel blocker [36]. Alternative explanations for the changes observed may be that (i) the peptide acts as a very slow open-channel blocker and therefore closings corresponding to blockages cannot be distinguished, (ii) the blocked channel can close, and (iii) the peptide blocks closed channels as described for many nAChR blockers [59–61]. Also, we cannot discard that the peptide acts by more than one mechanism and may enhance or stabilize desensitized states.

Interestingly, peptides corresponding to the neurotoxin-like region of the rabies virus glycoprotein inhibit macroscopic responses of α4β2 nAChRs with IC_{50} values in the high-micromolar range whereas the S peptide inhibits α7 with IC_{50} value in the low-micromolar range. Moreover, it was shown that the full length ectodomain of the rabies virus glycoprotein also inhibits nAChRs and that the peptides mediate in vivo effects in mice and *Caenorhabditis elegans* [11].

The identified interaction between the Y674-R685 peptide and α7 becomes important due to the increasing evidence showing the presence of free S and S1 proteins in body fluids. It has been proposed that after cleavage by furin there may be shedding of S1 during viral morphogenesis [62, 63] and that tissue damage may lead to free S protein and particles in plasma [64]. Moreover, it has been

hypothesized that inside the Open Reading Frame region of the S protein, the RNA polymerase can translate small neurotoxic peptides [65]. Our findings further add to the growing body of evidence that the free S protein may contribute to COVID-19 pathogenesis. Processes that are thought to be induced by S protein include thrombosis and blood coagulation [66], renal function abnormalities [67], impairment of vascular endothelial cells by down-regulation of ACE2 [68], and exacerbated pro-inflammatory responses through toll-like 2 signalling cascades in macrophages [69].

Thus, our work provides the impetus for further exploring interactions between α7 and S proteins, including those found in SARS-CoV-2 variants, such as the delta variant that carries a mutation (P681R) in the region herein studied.

Conclusions

Our results identify a functional interaction between a peptide corresponding to the Y674-R685 region of the SARS-CoV-2 S protein and the α7 nAChR. The S fragment exerts a dual effect on α7 nAChR, acting as an agonist in the presence of a PAM (silent agonist) and a non-competitive antagonist. It has been shown that activation of α7 nAChR in the immune system protects from excessive production of pro-inflammatory cytokines [14] and, therefore, impairment of this receptor results in an overproduction of cytokines and enhanced tissue damage [70]. Our finding raises the possibility that α7 nAChRs may be involved in the hyper-inflammatory response associated to COVID-19 and opens door for its further exploration.

Supplementary Information The online version contains supplementary material available at https://doi.org/10.1007/s12035-022-02947-8.

Acknowledgements We thank Dr. Franco Vizcarra (Oxford Brookes University) for helping with the whole-cell recordings.

Author Contribution JFC, ASFO, AJM, TG, IB, and CB designed the research; JFC, ASFO, IB, and CB performed the research and analysed the data; CB, ASFO, AJM, TG, JFC, and IB wrote, reviewed, and/or edited the paper. All authors read and approved the final manuscript.

Funding This work was supported by grants from Universidad Nacional del Sur (PGI 24/B298) and Agencia Nacional de Promoción Científica y Tecnológica (PICT 2017–1170) to CB and Oxford Brookes University (REA-2020) to IB. AJM and ASFO thank EPSRC (grant number EP/M022609/1) and BBSRC (grant number BB/R016445/1) for support. We thank BrisSynBio, a BBSRC/EPSRC Synthetic Biology Research Centre (Grant Number:BB/L01386X/1), for funding ASFO and providing funds to purchase the Y674-R685 peptide from Designer Bioscience Ltd. (Cambridge UK).

Data Availability The data that support the findings of this study are available within the article.

Declarations

Ethics Approval Not applicable.

Consent to Participate Not applicable.

Consent for Publication Not applicable.

Competing Interests The authors declare no competing interests.

References

1. Casalino L, Gaieb Z, Goldsmith JA et al (2020) Beyond shielding: the roles of glycans in the SARS-CoV-2 spike protein. ACS Cent Sci 6:1722–1734. https://doi.org/10.1021/acscentsci.0c01056
2. Hoffmann M, Kleine-Weber H, Schroeder S et al (2020) SARS-CoV-2 cell entry depends on ACE2 and TMPRSS2 and is blocked by a clinically proven protease inhibitor. Cell 181(2):271-280.e8. https://doi.org/10.1016/j.cell.2020.02.052
3. Yan R, Zhang Y, Li Y et al (2020) Structural basis for the recognition of SARS-CoV-2 by full-length human ACE2. Science 367(6485):1444–1448. https://doi.org/10.1126/science.abb2762
4. Cantuti-Castelvetri L, Ojha R, Pedro LD et al (2020) Neuropilin-1 facilitates SARS-CoV-2 cell entry and infectivity. Science 370(6518):856–860. https://doi.org/10.1126/science.abd2985
5. Daly JL, Simonetti B, Klein K et al (2020) Neuropilin-1 is a host factor for SARS-CoV-2 infection. Science 370(6518):861–865. https://doi.org/10.1126/science.abd3072
6. Changeux JP, Amoura Z, Rey FA, Miyara M (2020) A nicotinic hypothesis for Covid-19 with preventive and therapeutic implications. CR Biol 343(1):33–39. https://doi.org/10.5802/crbiol.8
7. Farsalinos K, Eliopoulos E, Leonidas DD et al (2020) Nicotinic cholinergic system and COVID-19: in silico identification of an interaction between SARS-CoV-2 and nicotinic receptors with potential therapeutic targeting implications. Int J Mol Sci 21(16):5807. https://doi.org/10.3390/ijms21165807
8. Oliveira A, Ibarra AA, Bermudez I et al (2021) A potential interaction between the SARS-CoV-2 spike protein and nicotinic acetylcholine receptors. Biophys J 120(6):983–993. https://doi.org/10.1016/j.bpj.2021.01.037
9. Grant SN, Lester H (2021) Regulation of epithelial sodium channel activity by SARS-CoV-1 and SARS-CoV-2 proteins. Biophys J 120(14):2805–2813. https://doi.org/10.1016/j.bpj.2021.06.005
10. Noviello CM, Gharpure A, Mukhtasimova N et al (2021) Structure and gating mechanism of the α7 nicotinic acetylcholine receptor. Cell 184(8):2121-2134.e13. https://doi.org/10.1016/j.cell.2021.02.049
11. Hueffer K, Khatri S, Rideout S et al (2017) Rabies virus modifies host behaviour through a snake-toxin like region of its glycoprotein that inhibits neurotransmitter receptors in the CNS. Sci Rep 7(1):12818. https://doi.org/10.1038/s41598-017-12726-4
12. Russo P, Bonassi S, Giacconi R et al (2020) COVID-19 and smoking: is nicotine the hidden link? Eur Respir J 55(6):2001116. https://doi.org/10.1183/13993003.01116-2020
13. Egea J, Buendia I, Parada E et al (2015) Anti-inflammatory role of microglial alpha7 nAChRs and its role in neuroprotection. Biochem Pharmacol 97(4):463–472. https://doi.org/10.1016/j.bcp.2015.07.032
14. Rosas-Ballina M, Ochani M, Parrish WR et al (2008) Splenic nerve is required for cholinergic antiinflammatory pathway control

of TNF in endotoxemia. Proc Natl Acad Sci USA 105(31):11008–11013. https://doi.org/10.1073/pnas.0803237105
15. Wang H, Yu M, Ochani M et al (2003) Nicotinic acetylcholine receptor alpha7 subunit is an essential regulator of inflammation. Nature 421(6921):384–388. https://doi.org/10.1038/nature01339
16. Pinheiro NM, Santana FP, Almeida RR et al (2017) Acute lung injury is reduced by the α7nAChR agonist PNU-282987 through changes in the macrophage profile. FASEB J: Off Publ Fed Am Soc Exp Biol 31(1):320–332. https://doi.org/10.1096/fj.201600431R
17. Wonnacott S (2014), Nicotinic ACh Receptors. Tocris Bioscience Scientific Reviews Series 1–31.
18. Nau J, Luthra P, Lanzer K et al (2021) Varenicline prevents SARS-CoV-2 infection in vitro and in Rhesus Macaques. bioRxiv [Preprint]. https://doi.org/10.1101/2021.06.29.450426 (accessed 20 September 2021).
19. Bouzat C, Bren N, Sine SM (1994) Structural basis of the different gating kinetics of fetal and adult nicotinic acetylcholine receptors. Neuron 13:1395–1402. https://doi.org/10.1016/0896-6273(94)90424-3
20. Chrestia JF, Bruzzone A, Esandi M, Bouzat C (2021) Tyrosine phosphorylation differentially fine-tunes ionotropic and metabotropic responses of human α7 nicotinic acetylcholine receptor. Cel Mol Life Sci: CMLS 78(13):5381–5395. https://doi.org/10.1007/s00018-021-03853-3
21. Gu S, Matta JA, Lord B et al (2016) Brain α7 nicotinic acetylcholine receptor assembly requires NACHO. Neuron 89(5):948–955. https://doi.org/10.1016/j.neuron.2016.01.018
22. Lansdell SJ, Gee VJ, Harkness PC et al (2005) RIC-3 enhances functional expression of multiple nicotinic acetylcholine receptor subtypes in mammalian cells. Mol Pharmacol 68(5):1431–1438. https://doi.org/10.1124/mol.105.017459
23. Lasala M, Fabiani C, Corradi J, Antollini S, Bouzat C (2019) Molecular modulation of human α7 nicotinic receptor by amyloid-β peptides. Front Cell Neurosci 13:37. https://doi.org/10.3389/fncel.2019.00037
24. Nielsen E, Bermudez I, Bouzat C (2019) Flavonoids as positive allosteric modulators of α7 nicotinic receptors. Neuropharmacology 160:107794. https://doi.org/10.1016/j.neuropharm.2019.107794
25. Andersen ND, Nielsen BE, Corradi J et al (2016) Exploring the positive allosteric modulation of human α7 nicotinic receptors from a single-channel perspective. Neuropharmacology 107:189–200. https://doi.org/10.1016/j.neuropharm.2016.02.032
26. Bouzat C, Bartos M, Corradi J, Sine SM (2008) The interface between extracellular and transmembrane domains of homomeric Cys-loop receptors governs open-channel lifetime and rate of desensitization. J Neurosci: Off J Soc Neurosci 28(31):7808–7819. https://doi.org/10.1523/JNEUROSCI.0448-08.2008
27. Andersen N, Corradi J, Sine SM, Bouzat C (2013) Stoichiometry for activation of neuronal α7 nicotinic receptors. Proc Natl Acad Sci USA 110(51):20819–20824. https://doi.org/10.1073/pnas.1315775110
28. Minguez-Viñas T, Nielsen BE, Shoemark DK et al (2021) A conserved arginine with non-conserved function is a key determinant of agonist selectivity in α7 nicotinic ACh receptors. Br J Pharmacol 178(7):1651–1668. https://doi.org/10.1111/bph.15389
29. Nielsen BE, Minguez T, Bermudez I, Bouzat C (2018) Molecular function of the novel α7β2 nicotinic receptor. Cel Mol Life Sci: CMLS 75(13):2457–2471. https://doi.org/10.1007/s00018-017-2741-4
30. Blunt CEW, Dougherty DA (2019) Binding interactions of NS6740, a silent agonist of the α7 nicotinic acetylcholine receptor. Mol Pharmacol 96(2):212–218. https://doi.org/10.1124/mol.119.116244
31. Chojnacka K, Papke RL, Horenstein NA (2013) Synthesis and evaluation of a conditionally-silent agonist for the α7 nicotinic acetylcholine receptor. Bioorg Med Chem Lett 23(14):4145–4149. https://doi.org/10.1016/j.bmcl.2013.05.039
32. Papke RL, Lindstrom JM (2020) Nicotinic acetylcholine receptors: conventional and unconventional ligands and signaling. Neuropharmacology 168:108021. https://doi.org/10.1016/j.neuropharm.2020.108021
33. daCosta CJ, Free CR, Corradi J, Bouzat C, Sine SM (2011) Single-channel and structural foundations of neuronal α7 acetylcholine receptor potentiation. J Neurosci: Off J Soc Neurosci 31(39):13870–13879. https://doi.org/10.1523/JNEUROSCI.2652-11.2011
34. Hurst RS, Hajós M, Raggenbass M et al (2005) A novel positive allosteric modulator of the alpha7 neuronal nicotinic acetylcholine receptor: in vitro and in vivo characterization. J Neurosci: Off J Soc Neurosci 25(17):4396–4405. https://doi.org/10.1523/JNEUROSCI.5269-04.2005
35. Zwart R, De Filippi G, Broad LM et al (2002) 5-Hydroxyindole potentiates human alpha 7 nicotinic receptor-mediated responses and enhances acetylcholine-induced glutamate release in cerebellar slices. Neuropharmacology 43(3):374–384. https://doi.org/10.1016/s0028-3908(02)00094-1
36. Neher E, Steinbach JH (1978) Local anaesthetics transiently block currents through single acetylcholine-receptor channels. J Physiol 277:153–176. https://doi.org/10.1113/jphysiol.1978.sp012267
37. Uteshev V (2014) The therapeutic promise of positive allosteric modulation of nicotinic receptors. Eur J Pharmacol 727:181–185. https://doi.org/10.1016/j.ejphar.2014.01.072
38. Dineley KT, Pandya AA (2015) Yakel JL (2015) Nicotinic ACh receptors as therapeutic targets in CNS disorders. Trends Pharmacol Sci 36(2):96–108. https://doi.org/10.1016/j.tips.2014.12.002
39. Yang T, Xiao T, Sun Q, Wang K (2017) The current agonists and positive allosteric modulators of α7 nAChR for CNS indications in clinical trials. Acta Pharmaceutica Sinica B 7(6):611–622. https://doi.org/10.1016/j.apsb.2017.09.001
40. Bouzat C, Lasala M, Nielsen BE, Corradi J, Esandi M (2018) Molecular function of α7 nicotinic receptors as drug targets. J Physiol 596(10):1847–1861. https://doi.org/10.1113/JP275101
41. Fucile S (2004) Ca2+ permeability of nicotinic acetylcholine receptors. Cell Calcium 35(1):1–8. https://doi.org/10.1016/j.ceca.2003.08.006
42. Fucile S (2017) The distribution of charged amino acid residues and the Ca2+ permeability of nicotinic acetylcholine receptors: a predictive model. Front Mol Neurosci. 10:155. Published 2017 May 29. https://doi.org/10.3389/fnmol.2017.00155
43. Changeux JP, Taly A (2008) Nicotinic receptors, allosteric proteins and medicine. Trends Mol Med 14(3):93–102. https://doi.org/10.1016/j.molmed.2008.01.001
44. Chatzidaki A, Millar NS (2015) Allosteric modulation of nicotinic acetylcholine receptors. Biochem Pharmacol 97(4):408–417. https://doi.org/10.1016/j.bcp.2015.07.028
45. Bertrand D, Gopalakrishnan M (2007) Allosteric modulation of nicotinic acetylcholine receptors. Biochem Pharmacol 74(8):1155–1163. https://doi.org/10.1016/j.bcp.2007.07.011
46. Grønlien JH, Håkerud M, Ween H et al (2007) Distinct profiles of alpha7 nAChR positive allosteric modulation revealed by structurally diverse chemotypes. Mol Pharmacol 72(3):715–724. https://doi.org/10.1124/mol.107.035410
47. Papke RL, Bagdas D, Kulkarni AR et al (2015) The analgesic-like properties of the alpha7 nAChR silent agonist NS6740 is associated with non-conducting conformations of the receptor. Neuropharmacology 91:34–42. https://doi.org/10.1016/j.neuropharm.2014.12.002
48. Guan YZ, Jin XD, Guan LX et al (2015) Nicotine inhibits microglial proliferation and is neuroprotective in global ischemia

rats. Mol Neurobiol 51(3):1480–1488. https://doi.org/10.1007/s12035-014-8825-3
49. Kabbani N, Nordman JC, Corgiat BA et al (2013) Are nicotinic acetylcholine receptors coupled to G proteins. BioEssays: News Rev Mol Cel Dev Biol 35(12):1025–1034. https://doi.org/10.1002/bies.201300082
50. Godin JR, Roy P, Quadri M et al (2020) A silent agonist of α7 nicotinic acetylcholine receptors modulates inflammation ex vivo and attenuates EAE. Brain Behav Immun 87:286–300. https://doi.org/10.1016/j.bbi.2019.12.014
51. Mukhtasimova N, Lee WY, Wang HL, Sine SM (2009) Detection and trapping of intermediate states priming nicotinic receptor channel opening. Nature 459(7245):451–454. https://doi.org/10.1038/nature07923
52. Brams M, Gay EA, Sáez JC et al (2011) Crystal structures of a cysteine-modified mutant in loop D of acetylcholine-binding protein. J Biol Chem 286(6):4420–4428. https://doi.org/10.1074/jbc.M110.188730
53. Hansen SB, Sulzenbacher G, Huxford T et al (2005) Structures of Aplysia AChBP complexes with nicotinic agonists and antagonists reveal distinctive binding interfaces and conformations. EMBO J 24(20):3635–3646. https://doi.org/10.1038/sj.emboj.7600828
54. Hibbs RE, Sulzenbacher G, Shi J et al (2009) Structural determinants for interaction of partial agonists with acetylcholine binding protein and neuronal alpha7 nicotinic acetylcholine receptor. EMBO J 28(19):3040–3051. https://doi.org/10.1038/emboj.2009.227
55. Fabiani C, Murray AP, Corradi J, Antollini SS (2018) A novel pharmacological activity of caffeine in the cholinergic system. Neuropharmacology 135:464–473. https://doi.org/10.1016/j.neuropharm.2018.03.041
56. Pereira EF, Hilmas C, Santos MD et al (2002) Unconventional ligands and modulators of nicotinic receptors. J Neurobiol 53(4):479–500. https://doi.org/10.1002/neu.10146
57. Spurny R, Debaveye S, Farinha A et al (2015) Molecular blueprint of allosteric binding sites in a homologue of the agonist-binding domain of the α7 nicotinic acetylcholine receptor. Proc Natl Acad Sci USA 112(19):E2543–E2552. https://doi.org/10.1073/pnas.1418289112
58. Young GT, Zwart R, Walker AS, Sher E, Millar NS (2008) Potentiation of alpha7 nicotinic acetylcholine receptors via an allosteric transmembrane site. Proc Natl Acad Sci USA 105(38):14686–14691. https://doi.org/10.1073/pnas.0804372105
59. Bouzat CB, Barrantes FJ (1996) Modulation of muscle nicotinic acetylcholine receptors by the glucocorticoid hydrocortisone. J Biol Chem 271(42):25835–25841. https://doi.org/10.1074/jbc.271.42.25835
60. Dilger JP, Brett RS (1991) Actions of volatile anesthetics and alcohols on cholinergic receptor channels. Ann N Y Acad Sci 625:616–627. https://doi.org/10.1111/j.1749-6632.1991.tb33896.x
61. Dilger JP, Boguslavsky R, Barann M, Katz T, Vidal AM (1997) Mechanisms of barbiturate inhibition of acetylcholine receptor channels. J Gen Physiol 109(3):401–414. https://doi.org/10.1085/jgp.109.3.401
62. Letarov AV, Babenko VV, Kulikov EE (2021) Free SARS-CoV-2 spike protein S1 particles may play a role in the pathogenesis of COVID-19 infection. Biochemistry (Mosc) 86(3):257–261. https://doi.org/10.1134/S0006297921030032
63. Zhang L, Jackson CB, Mou H, et al (2020) The D614G mutation in the SARS-CoV-2 spike protein reduces S1 shedding and increases infectivity. Preprint. bioRxiv. 2020.06.12.148726. Published 2020 Jun 12. https://doi.org/10.1101/2020.06.12.148726
64. Ogata AF, Maley AM, Wu C et al (2020) Ultra-sensitive serial profiling of SARS-CoV-2 antigens and antibodies in plasma to understand disease progression in COVID-19 patients with severe disease. Clin Chem 66(12):1562–1572. https://doi.org/10.1093/clinchem/hvaa213
65. Cafiero C, Micera A, Re A et al (2021) Could small neurotoxins-peptides be expressed during SARS-CoV-2 infection? Curr Genomics 22(8):557–563. https://doi.org/10.2174/1389202922666211221111527
66. Zheng Y, Zhao J, Li J et al (2021) SARS-CoV-2 spike protein causes blood coagulation and thrombosis by competitive binding to heparan sulfate. Int J Biol Macromol 193(Pt B):1124–1129. https://doi.org/10.1016/j.ijbiomac.2021.10.112Z
67. George S, Pal AC, Gagnon J et al (2021) Evidence for SARS-CoV-2 spike protein in the urine of COVID-19 patients. Kidney360 2(6):924–936. https://doi.org/10.34067/KID.0002172021
68. Lei Y, Zhang J, Schiavon CR, He M, Chen L, Shen H, Zhang Y, Yin Q et al (2021) SARS-CoV-2 spike protein impairs endothelial function via downregulation of ACE 2. Circ Res 128(9):1323–1326. https://doi.org/10.1161/CIRCRESAHA.121.318902
69. Shirato K, Kizaki T (2021) SARS-CoV-2 spike protein S1 subunit induces pro-inflammatory responses via toll-like receptor 4 signaling in murine and human macrophages. Heliyon. 7(2):e06187. Published 2021 Feb 2. https://doi.org/10.1016/j.heliyon.2021.e06187
70. Parrish WR, Rosas-Ballina M, Gallowitsch-Puerta M et al (2008) Modulation of TNF release by choline requires alpha7 subunit nicotinic acetylcholine receptor-mediated signaling. Molecular medicine (Cambridge, Mass.) 14(9–10) 567–574. https://doi.org/10.2119/2008-00079.Parrish